JACS
JOURNAL OF THE AMERICAN CHEMICAL SOCIETY

Article

pubs.acs.org/JACS

Unique Proton Dynamics in an Efficient MOF-Based Proton Conductor

Yong-Sheng Wei,[†] Xiao-Peng Hu,[†] Zhen Han,[†] Xi-Yan Dong,[†] Shuang-Quan Zang,*[,†] and Thomas C. W. Mak[†,‡]

[†]College of Chemistry and Molecular Engineering, Zhengzhou University, Zhengzhou 450001, China

[‡]Department of Chemistry and Center of Novel Functional Molecules, The Chinese University of Hong Kong, Shatin, New Territories, Hong Kong SAR, China

Supporting Information

ABSTRACT: Recently, research on metal−organic frameworks (MOFs) serving as a new type of proton conductive material has resulted in many exciting achievements. However, direct observation of a well-established proton-transfer mechanism still remains challenging in MOFs and other crystalline compounds, let alone other conductive materials. Herein we report the solvothermal synthesis of a new proton-conducting MOF, $(Me_2NH_2)[Eu(L)]$ (H_4L = 5-(phosphonomethyl)isophthalic acid). The compound consists of a layered anionic framework $[Eu(L)]^-$ and interlayer-embedded counter cations $(Me_2NH_2)^+$, which interact with adjacent uncoordinated O atoms of phosphonate groups to form strongly (N−H···O) hydrogen-bonded chains aligned parallel to the *c*-axis. Facile proton transfer along these chains endows the compound with single-crystal anhydrous conductivity of 1.25×10^{-3} S·cm^{-1} at 150 °C, and water-assisted proton conductivity for a compacted pellet of microcrystalline crystals attains 3.76×10^{-3} S·cm^{-1} at 100 °C and 98% relative humidity (RH). Proton dynamics (vibrating and transfer) within N−H···O chains of the compound are directly observed using a combination of anisotropic conductivity measurements and control experiments using large single-crystals and pelletized samples, in situ variable-temperature characterization techniques including powder X-ray diffraction (PXRD), single-crystal X-ray diffraction (SCXRD), diffuse reflectance infrared Fourier transform spectrum (DRIFTS), and variable-temperature photoluminescence. In particular, a scarce single-crystal to single-crystal (SCSC) transformation accompanied by proton transfer between an anionic structure $(Me_2N\mathbf{H}_2)[Eu(L)]$ and an identical neutral framework $[Eu(\mathbf{H}L)]$ has been identified.

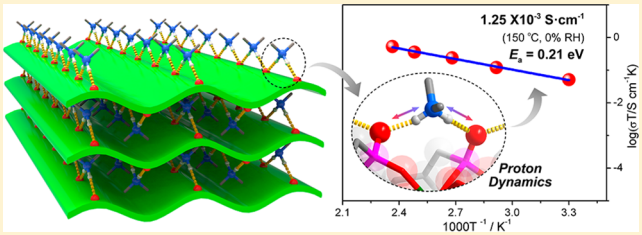

INTRODUCTION

Clean energy production is one of the most challenging targets for sustainable energy development. Fuel cells, as very promising candidates, have accelerated the continuous exploration of novel proton conductors.[1] Metal−organic frameworks (MOFs) or porous coordination polymers (PCPs), possessing large surface areas and highly ordered structures, have demonstrated their superiority in gas storage/separation,[2] luminescence,[3] catalysis,[4] and other fields of application.[5] As a relatively new type of conducting material, MOFs have also drawn increased attention because their modular building blocks endow them with diversity and functional adjustability, and high crystallinity makes them suitable platforms to well understand the operating mechanism of proton transfer.[6]

To date, MOFs with high humidity conductivities have been widely prepared,[7,8] but their operation usually relies critically on the presence of water molecules and ceases to function at temperatures above 100 °C. Considering that physical properties, e.g., magnetism and photoluminescence, of MOFs can be well modulated by guest molecules,[3f,9] excellent proton conductivities at high temperature (>100 °C) might be realized when nonvolatile proton carriers such as H_2SO_4, H_3PO_4, imidazole, triazole, NH_4^+, and $(Me_2NH_2)^+$ are encapsulated in their cavities or defect sites, and actually this kind of new high-performance proton conductor has been observed in many cases.[10] However, the synthesis of MOFs possessing intrinsic high proton conductivities under both humid atmospheric and high-temperature anhydrous conditions, especially at temperatures above 120 °C, still remains a challenging problem.[7g,11]

In keeping with the preparative development of proton-conducting MOFs, the detailed proton conduction mechanism needs to be elucidated, which can direct the rational design of superior MOF proton conductors functioning over a wide range of temperatures and under both aqueous and anhydrous environments. A variety of characterization approaches, such as water adsorption, anisotropic conductivities of measurement, and X-ray crystallography, have been employed to investigate the mechanism of proton transfer.[8a−e,10h] Very recently, computer simulations and quasi-elastic neutron scattering (QENS) were also utilized to elucidate the proton transport

Received: December 14, 2016
Published: February 14, 2017

DOI: 10.1021/jacs.6b12847
J. Am. Chem. Soc. 2017, 139, 3505−3512

mechanism in a humid atmosphere.[2d,8a,12] However, direct observation of well-established proton transfer in MOF-based conductors by a hopping (relay) mechanism using in situ characterization methods including single-crystal X-ray diffraction (SCXRD) analysis still face challenges, because it demands harsh terms, for instance inherent high conductivity, easy proton transfer under accessible conditions, large single-crystal growth to avoid pelleted measurement,[8d,13] and maintenance of high crystallinity at elevated temperatures. Visual single-crystal to single-crystal (SCSC) transformation accompanied by proton transfer among different groups is very desirable for elucidating proton conduction pathway, but thus far it has not been realized. For the foregoing reasons, to capture the intermediate and final states by SCXRD and other related in situ characterization techniques presents a significant challenge.

Herein we report a new highly thermal- and water-stable layered MOF, $(Me_2NH_2)[Eu(L)]$ (**1**), in which strongly hydrogen-bonded (N−H···O) chains between $(Me_2NH_2)^+$ and phosphonate groups of the anionic host framework are orderly assembled in the interlayer region, which manifests high-performance proton conductivities under both anhydrous and water-assisted conditions. More importantly, because MOF **1** retains its good single crystallinity at high temperature, the proton transfer mechanism of the compound was elucidated by a series of in situ variable-temperature characterization techniques including SCXRD, IR, powder X-ray diffraction (PXRD), and photoluminescence, as well as controlled experiments including a scarce SCSC transformation accompanied by proton transfer between an anionic framework and an identical neutral framework. All results confirmed that unique proton vibration and transfer between the $(Me_2NH_2)^+$ cations and the phosphonate groups of the host framework were realized by virtue of strong hydrogen-bonding and electrostatic interactions, which contributes to the inherently high proton conductivity.

EXPERIMENTAL SECTION

Preparation of $(Me_2NH_2)[Eu(L)]$ (1). A mixture of $Eu(NO_3)_3\cdot 6H_2O$ (8.9 mg, 0.020 mmol), H_4L (7.8 mg, 0.03 mmol), NaOH (4.8 mg, 0.12 mmol), and DMF−H_2O solution (1:1, 2.0 mL) was sealed in a 23 mL Teflon-lined stainless steel container, heated at 160 °C for 3 days, and then cooled to room temperature. Colorless single crystals of $(Me_2NH_2)[Eu(L)]$ were isolated. Yield 61% (based on Eu). Elemental analyses (%) for **1** ($C_{11}H_{13}NO_7EuP$): Calcd C 29.09, H 2.89, N 3.08. Found C 29.05, H 2.83, N 3.07. IR (Figure S5, KBr pellet, ν/cm^{-1}): 3418 (w), 3065 (w), 3014 (w), 2930 (w), 2901 (w), 2704 (m), 2656 (m), 2400 (m), 2197 (m), 1898 (w), 1859 (m), 1630 (s), 1609 (s), 1545 (vs), 1445 (s), 1380 (vs), 1220 (m), 1147 (m), 1107 (vs), 1173 (vs), 1000 (vs), 953 (s), 915 (m), 785 (s), 756 (m), 707 (m), 685 (m), 614 (m) 536 (vs), 482 (m).

Preparation of [Eu(HL)] (1a). When **1** was heated to 450 °C at a rate of 0.5 °C·min^{-1} in a N_2 stream for 15 min, **1a** was obtained. Elemental analyses (%) for **1a** ($C_9H_6O_7EuP$): Calcd C 26.42, H 1.48, N 0.00. Found C 26.69, H 1.45, N 0.00. IR (Figure S5, KBr pellet, ν/cm^{-1}): 3418 (m), 3280 (m), 2922 (w), 1852 (s), 1621 (s), 1528 (vs), 1450 (s), 1380 (vs), 1228 (w), 1171 (s), 1117 (vs), 961 (w), 905 (s), 793 (m), 773 (w), 758 (w), 705 (m), 678 (m), 614 (m) 527 (s), 471 (m).

Preparation of $(Me_2NH_2)_{0.6}[Eu(L)_{0.6}(HL)_{0.4}]\cdot 0.4H_2O$ (1′). **1a** (15.0 mg, 0.037 mmol) was added into an aqueous Me_2NH solution (0.15 mmol Me_2NH in 6.0 mL water), which was sealed in a 23 mL Teflon-lined stainless steel container and then heated at 160 °C for 12 h, resulting in the formation of **1′**. Elemental analyses (%) for **1′** ($C_{10.2}H_{11}N_{0.6}O_{7.4}EuP$): Calcd C 27.63, H 2.50, N 1.90. Found C 24.90, H 2.39, N 1.87. IR (Figure S5, KBr pellet, ν/cm^{-1}): 3473 (m), 3073 (w), 3014 (w), 2932 (w), 2899 (w), 2703 (m), 2648 (m), 2400 (m), 2207 (m), 1857 (m), 1627 (s), 1609 (s), 1539 (vs), 1447 (s), 1374 (vs), 1223 (m), 1151 (m), 1116 (vs), 1073 (vs), 1004 (vs), 962 (m), 912 (m), 793 (s), 782 (m), 708 (m), 685 (m), 626 (w) 540 (s), 485 (m).

Test of Exchange with Ammonium Analogues. The experiments were carried out by adding **1** (9.0 mg, 0.02 mmol) and 0.04 mmol of an ammonium analogue ($Et_2NH\cdot HCl$, $MeNH_2\cdot HCl$ and NH_4Cl separately) into water (6.0 mL) and then heating at 160 °C for 3 days. The PXRD patterns (Figure S6) and EA results (Table S1) of these samples agreed well with those of **1**, implying that the strong hydrogen-bonded chains remain intact and the $(Me_2NH_2)^+$ cation is not replaced by other ammonium analogues.

Calculation of Thermal Expansion Coefficients. The linear thermal expansion coefficient α was calculated by

$$\alpha = \partial f(T)/\partial T \times 1/f(T)$$

where T is the temperature, and $f(T)$ is the temperature-dependent unit-cell parameter of interest, which was fitted by a suitable linear equation:

$$f(T) = a_0 + a_1 T$$

Single-Crystal X-ray Diffraction Analysis. Diffraction measurements were performed on a Rigaku XtaLAB Pro diffractometer with Mo Kα radiation (λ = 0.71073 Å) for **1** at variable temperatures, and Cu Kα radiation (λ = 1.54184 Å) for **1′** at 200 K. SCXRD data of **1a** was collected with Mo Kα radiation (λ = 0.71073 Å) on a Bruker D8 VENTURE diffractometer at room temperature. All structures were solved by the direct method and refined by full-matrix least-squares on F^2 using the SHELXTL-2013 package. All non-hydrogen atoms were refined anisotropically. The hydrogen atoms (H1a and H1b) attached to N atom of $(Me_2NH_2)^+$ were located from difference Fourier maps, and their positions were freely refined with isotropic thermal displacement parameters fixed at 1.2 times U_{eq} of their parent N atom. Fourier difference maps ($F_0 - F_c$) in bitmap and contour styles were both computed with the WinGX program system. Other hydrogen atoms were placed in geometrically generated positions. Detailed structure refinement parameters and crystallographic data are given in Table S7.

RESULTS AND DISCUSSION

Syntheses and Characterization. Solvothermal reaction of $Eu(NO_3)_3$, H_4L, and NaOH in H_2O−DMF (DMF = *N*,*N*-dimethylformamide) yielded colorless block-like crystals of $(Me_2NH_2)[Eu(L)]$ (**1**). SCXRD analysis showed that its asymmetric unit (space group $P2_1/c$) consists of one Eu(III) ion, one L^{4-} ligand, and one $(Me_2NH_2)^+$ ion (Figure S1) which results from thermal decomposition of the DMF molecule. Each Eu(III) center is coordinated octahedrally by four carboxylate O atoms of four L^{4-} ligands and two phosphonate O atoms of two other L^{4-} ligands. Each L^{4-} ligand coordinates with six Eu(III) ions by four O atoms from two carboxylate groups and two O atoms from one phosphate group, leaving one uncoordinated O atom (O7). This gives rise to a wavy-layered architecture, which can be considered to be composed of countless edge-shared ring units (along the *bc* plane) with L^{4-} ligands located in its central regions (Figures 1a and S2). If both Eu(III) and L^{4-} are considered as 6-connected nodes, the layered structure can be simplified as a new binodal 6,6-connected network with point symbol $\{4^{15}\}$.[14]

The anionic host framework constructed by the interconnection of $[Eu(L)]^-$ units is charge-balanced by the periodically aligned $(Me_2NH_2)^+$ cations that occupy the interlayer region (Figures 1b and S3). Interestingly, a view down the *c*-axis shows zigzag hydrogen-bonded (N−H···O) chains each assembled by

DOI: 10.1021/jacs.6b12847
J. Am. Chem. Soc. 2017, 139, 3505−3512

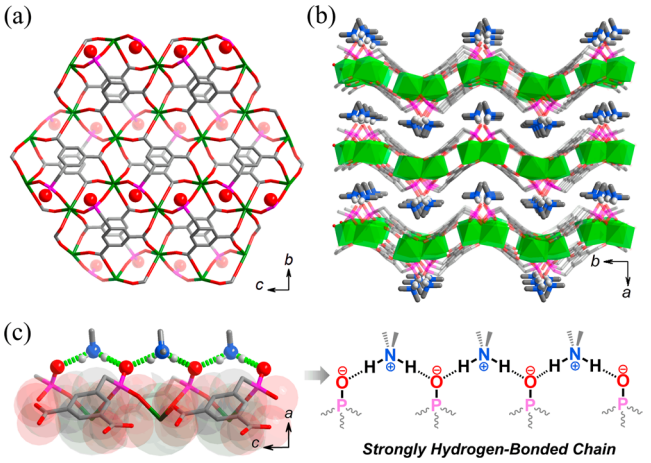

Figure 1. (a) Perspective views of the layer anionic host framework of **1** along the *a*-axis (the uncoordinated O atoms of phosphonate groups are shown as red spheres) and (b) the sandwich-type structure of **1** along the *c*-axis with the counter cations $(Me_2NH_2)^+$ periodically aligned in the interlayers. (c) Strongly hydrogen-bonded (N−H···O) chain assembled alternately by $(Me_2NH_2)^+$ cations and uncoordinated oxygen (O7) atoms of phosphonate groups of the anionic host framework.

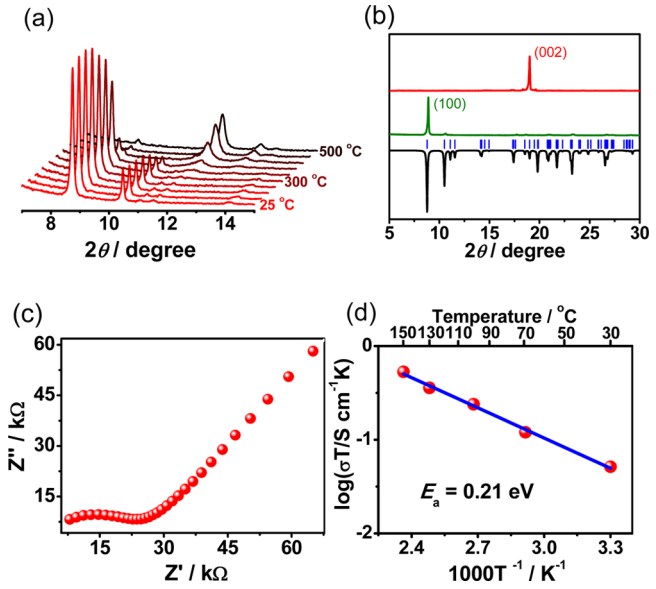

Figure 2. (a) In situ variable-temperature PXRD patterns of **1** under N_2 atmosphere. (b) PXRD patterns of simulation (black), a large single-crystal of **1** relative to the *bc* plane (green) and the *ab* plane (red). (c) Nyquist plot of **1** at 150 °C and (d) Arrhenius plot of conductivities of **1** from 30 to 150 °C under anhydrous conditions along the *c*-axis.

linking an alternate arrangement of $(Me_2NH_2)^+$ cations and O7 atoms of phosphonate groups (Figures 1c and S4). Importantly, the hydrogen-bonded N−H_2 groups can be confirmed by two strong and wide IR spectral bands ν_1 (2000−2550 cm^{-1}) and ν_2 (2550−2800 cm^{-1}) (Figure S5),[15] which are significantly lower than 2800 cm^{-1} for normal hydrogen-bonded N−H stretching vibrations.[7g,11,16] Judging from the different distances between donor (N1) and acceptor (O7) atoms for H1a (2.693(2) Å) and H1b (2.716(2) Å), spectral bands ν_1 and ν_2 can be ascribed to the hydrogen-bonded N−H1a and N−H1b stretching vibrations, respectively. In addition, it has been demonstrated that the hydrogen-bonded chain retains its integrity in the presence of ammonium analogues (Figure S6 and Table S1). In brief, strongly hydrogen-bonded chains constructed by optimal acid−base pairing has yielded a crystalline material that holds promise as a good proton conductor.[11]

Prior to proton conductivity measurements, the thermal and water stability of **1** were investigated.[17] Thermogravimetric analyses (TGA) and differential scanning calorimetry (DSC) showed that **1** can be thermally stable up to 300 °C (Figures S7 and S8), which was also determined by variable-temperature PXRD (Figure 2a). Furthermore, PXRD patterns of samples soaked in water for six months or boiled in water for 2 weeks did not differ from that of an as-synthesized sample (Figures S9 and S10), indicating that **1** is an excellent thermal- and water-stable crystalline material. In a word, the unique structural characteristics and high thermal and water stabilities of **1** make it a promising candidate as an excellent proton-conducting material under both anhydrous and humid conditions.

Proton Conductivities under Anhydrous Conditions. In view of the plentiful strongly hydrogen-bonded chains periodically aligned along the crystallographic *c*-axis in **1**, alternating current (AC) impedance measurements were first performed on a selected large single crystal with dimensions of about 0.32 mm × 0.29 mm × 0.26 mm. With the single-crystal orientation determined by PXRD, only one diffraction, indexed as (002), was observed, which identified the *c*-axis as the orientation direction of the hydrogen-bonded chains (Figure 2b). By attaching gold-pasted electrodes to both identified sides of the single crystal,[13c] AC conductivities were measured at 30−150 °C under anhydrous conditions (N_2 atmosphere), and the real (Z') and imaginary (Z'') parts of the impedance spectrum are shown in Figure 2c. The impedance plots could be excellently fitted by a designed equivalent resistor−capacitor (RC) circuit, and the tail at low frequencies should correspond to diffusion impedance (Figure S12). At 30 °C, the proton conductivity of a single-crystal sample was 1.69×10^{-4} S·cm^{-1}, reaching a maximum of 1.25×10^{-3} S·cm^{-1} at 150 °C (Figure S13), which is higher than those of phosphate/sulfonate-based MOFs, such as *β*-PCMOF2$(Tz)_{0.3}$,[10g] $[Zn(HPO_4)(H_2PO_4)_2]\cdot 2H_2Im$,[18] $[(Me_2NH_2)_3(SO_4)]_2[Zn_2(o\ x)_3]$,[11] and $[Zn(H_2PO_4)_2(TzH)_2]$,[13d] and comparable to those of $[ImH_2][Cu(H_2PO_4)_2Cl]\cdot H_2O$[19] and $[Zn_3(H_2PO_4)_6(H_2\ O)_3]\cdot$Hbim.[20] Just as expected, no proton conductivities exist through other crystal faces under similar conditions (Figure S14), which further proves that efficient proton transfer occurs solely along the hydrogen-bonded chains. The proton transfer activation energy (E_a) for a single crystal of **1** along the *c*-axis was calculated to be 0.21 eV (Figure 2d) according to the least-squares fit of an Arrhenius plot, which is close to the lowest value reported for proton-conductive MOFs under anhydrous conditions (Figure S15 and Table S2), and only behind one MOF $[(Me_2NH_2)_3(SO_4)]_2[Zn_2(ox)_3]$ reported by the Ghosh group.[11] Such a low activation value means that proton conduction in **1** belongs to the Grotthuss (hopping) mechanism (<0.4 eV), which further supports that the strongly hydrogen-bonded chains constructed by acid−base pairs in **1** can yield facile and efficient proton transfer with the help of electrostatic interactions.[11] In contrast, AC impedance measurements of **1** using a compacted pellet of microcrystalline crystals exhibit extremely poor proton conductivity in the range of 10^{-8} to 10^{-7} S·cm^{-1} even at 150 °C under dry N_2 atmosphere, which is possibly attributable to big grain boundary resistance under N_2 atmosphere; in other words,

DOI: 10.1021/jacs.6b12847
J. Am. Chem. Soc. 2017, 139, 3505−3512

hydrogen-bonded chains cannot link up cooperatively among microcrystalline crystals in the compacted pellet under this condition.

Proton Conductivities under Different Humid Conditions. The distinctly different proton conductivities between a large single crystal and a pellet suggested to us that water molecules may serve as bridges to establish a way for proton transfer among the microcrystalline crystals in the pellet. To confirm this conjecture, AC impedance measurements under different humid conditions were performed. It should be first noted that, although **1** is a nonporous structure, the pellet sample of **1** can exhibit good capacity for water storage, showing water vapor uptake six times (48.3 $cm^3 \cdot g^{-1}$) that of its dispersed sample (8.13 $cm^3 \cdot g^{-1}$) (Figure S11), possibly due to abundant small interstices generated in the pellet sample. Compared with the proton conductivity of single-crystal sample, the impedance plots for the pellet sample could be fitted well by two serial equivalent RC circuits (Figure S16), in which one RC circuit was assigned to the bulk phase, and the other to the grain boundaries.[21] By comparing the range of frequencies showing relaxation processes and their activation energy (0.38 and 0.74 eV, respectively) of R_1 and R_2,[21] and considering the results of single-crystal samples, the smaller one (R_1) in relative high frequency should be attributed to bulk resistance, and the larger one (R_2) may be grain-boundary resistance, respectively. Furthermore, the values of (R_1 + R_2) were considered as the resistance of a pellet. The linear region of the Nyquist plots also resulted from an ion-blocking at the electrodes which, combined with DC conductivity of **1**, definitely excludes the possibility of electronic conduction (Figure S17).[21b] Under 98% relative humidity (RH), the proton conductivities for the pellet of **1** at 30 and 100 °C were 2.17×10^{-5} and 3.76×10^{-3} $S \cdot cm^{-1}$, respectively (Figure S18). In particular, the value of 3.76×10^{-3} $S \cdot cm^{-1}$ is the highest conductivity reported among MOF materials, even higher than those of Cu-DOSA (1.9×10^{-3} $S \cdot cm^{-1}$ at 85 °C and 98% RH),[22] PCMOF-5 (2.5×10^{-3} $S \cdot cm^{-1}$ at 60 °C and 98% RH),[8e] and In-IA-2D-1 (3.4×10^{-3} $S \cdot cm^{-1}$ at 27 °C and 98% RH),[7g] being comparable to those of $PCMOF2_{1/2}$ (2.1×10^{-2} $S \cdot cm^{-1}$ at 85 °C and 90% RH)[23] and $[(Me_2NH_2)_3(SO_4)]_2[Zn_2(ox)_3]$ (4.2×10^{-2} $S \cdot cm^{-1}$ at 25 °C and 98% RH).[11] The activation energy for the pellet of **1** at 98% RH was evaluated as 0.72 eV, respectively, which should belong to a combination of Grotthuss (hopping) (< 0.4 eV) and vehicle mechanism (> 0.4 eV), indicating that numerous water molecules (mobile proton carriers) effectively bridge adjacent microcrystalline crystals in the compacted pellet to transport protons. In addition, we tried to use compound **1** as a solid-state electrolyte to assemble a H_2/O_2 fuel cell (Figure S19), which gives a maximum open circuit voltage (OCV) of 0.87 V at 80 °C, 98% RH (Figure S20), similar to those reported in the literature.[10a,24]

Proton Vibration within the (N−H···O) Hydrogen Bond. The inherent high conductivity and excellent thermal stability of **1** further prompted us to investigate the type of hydrogen-bonded chain and even the positions of protons. In situ SCXRD at different temperatures showed that, over a span of 300 K, there are significant variations of a by 1.2% for **1**, corresponding to an average thermal expansion coefficient of α_a = 41.3 ppm K^{-1}, which is ca. 8 and 5 times larger than those of the b (4.9 ppm K^{-1}) and c (−8.3 ppm K^{-1}) axes, respectively (Figure S21 and Table S3).[4g,25] Careful structural analysis supports that the anisotropic changes of unit-cell parameters arise from supramolecular interaction between 2D anion frameworks and dynamic $(Me_2NH_2)^+$ cations,[25b,26] which reveal more severe vibration than that of 2D anion host frameworks (Figure S22 and Table S4). Actually, this drastic vibrational behavior may facilitate dynamic transfer of protons along the hydrogen-bonded (N−H···O) chain.[10f,h,18]

As is well-known, when the included guest molecules are strongly confined within a host framework of high crystallinity,[26c,27] proton dynamics within strong hydrogen bonds can be visualized at the molecular/atom level by SCXRD.[26a,28] In the case of **1**, the electron-density distribution of the hydrogen-bonded hydrogen atoms (H1a and H1b) of $(Me_2N\mathbf{H_2})^+$ can be clearly observed in X-ray difference Fourier maps (Figures 3a,

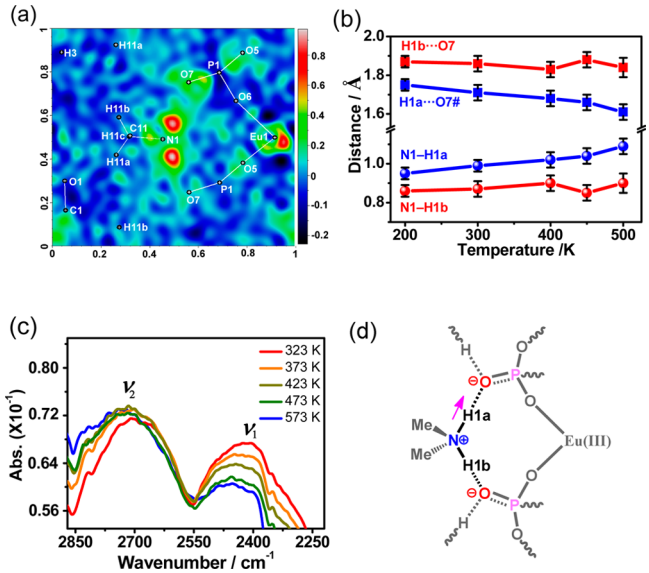

Figure 3. (a) X-ray difference Fourier map in the region of the $(Me_2NH_2)^+$ and phosphate groups of **1**. (b) Variation of hydrogen-bond (N−H···O) distances of **1** at different temperatures. (c) Temperature-dependent DRIFTS spectra for **1** under N_2 atmosphere. (d) Sufficiently high temperature would eventually lead to breakage of one N−H bond of $(Me_2NH_2)^+$ cation, and thus the phosphate groups should accept the protons to maintain electric neutrality of **1**.

S23 and S24). Excitingly, in situ SCXRD measurements showed that, as temperature increases, the H1a atom gradually moves away from its parent N1 atom, while the N1−H1b bond length remains almost unchanged (Figure 3b). Importantly, such peculiar behavior is well repeated during the heating−cooling cycle (Table S5). Besides these, considering the fact that low electron density of the H atom hardly provides an accurate determination of the positions of all H1a and H1b atoms in the single crystal of **1**, a more subtle investigation of proton dynamical behavior needs to draw support from other characterization methods, e.g., IR spectra.[29] As mentioned above, the wide spectral bands ν_1 and ν_2 can be ascribed to the hydrogen-bonded N−H1a and N−H1b stretching vibrations, respectively.[15] When temperature rises from 298 to 573 K, the in situ diffuse reflectance infrared Fourier transform spectrum (DRIFTS) shows that both ν_1 and ν_1 gradually shift to higher frequencies at varying degrees (Figure 3c), probably resulting from weakening of the hydrogen bonds at high temperatures (Table S5),[29b,30] which even overwhelms the red-shift influence caused by elongation of the N−H1a bond. Additionally, as the temperature rises, DRIFTS spectra showed that the absolute

DOI: 10.1021/jacs.6b12847
J. Am. Chem. Soc. 2017, 139, 3505−3512

intensity of ν_1 gradually decreases while ν_2 remains almost unchanged, suggesting a probable reduction in the number of H1a atoms attached to N centers; that is, some of the H1a atoms may shuttle between the donor (N1) and acceptor (O7) atoms at high temperatures, although this hypothetical behavior is not observable in X-ray difference Fourier maps. The above phenomena seem to indicate that sufficiently high temperature would eventually lead to loss of one H^+ from N−H_2 of $(Me_2NH_2)^+$ cations. In this way, the proton acceptor, namely a phosphate group of the host framework, can maintain the electric neutrality of **1** (Figure 3d). This hypothesis has been confirmed by subsequent SCXRD, X-ray photoelectron spectroscopy (XPS), IR, and luminescent measurements.

Proton Transfer from $(Me_2NH_2)^+$ Cations to O_3P Groups. Because high temperature induces stretching of the N−H1a bond in $(Me_2NH_2)^+$, sufficiently high energy would promote H^+ transfer to the O sites of PO_3 groups. As the boiling point of Me_2NH is only 7.4 °C, it would easily escape from **1** after its incorporation. As expected, TGA showed that **1** gives a weight loss of 9.7% from 350 to 450 °C (Figure S7), which can be attributed to Me_2NH molecules (calcd: 9.9%) from deprotonated $(Me_2NH_2)^+$ lattice cations, finally yielding a new phase (**1a**), which was also verified by variable-temperature PXRD (Figures 2a and S25). Elemental analyses (EA) and XPS showed the absence of N atoms in **1a**, implying that all Me_2NH molecules have successfully escaped from **1** (Figures 4a and S26). Another crucial information provided by XPS is that the valence state of the Eu(III) ion in **1a** is consistent with that of **1** (Figure S26c). Besides, compared with **1**, the two strong and wide IR spectral bands ν_1 and ν_2 in **1a** completely disappeared, while the 3280 cm^{-1} peak referring to PO-H, appeared (Figures 4b and S5),[31] indicating acidification of PO_3 groups and the presence of PO_3H after Me_2NH removal.

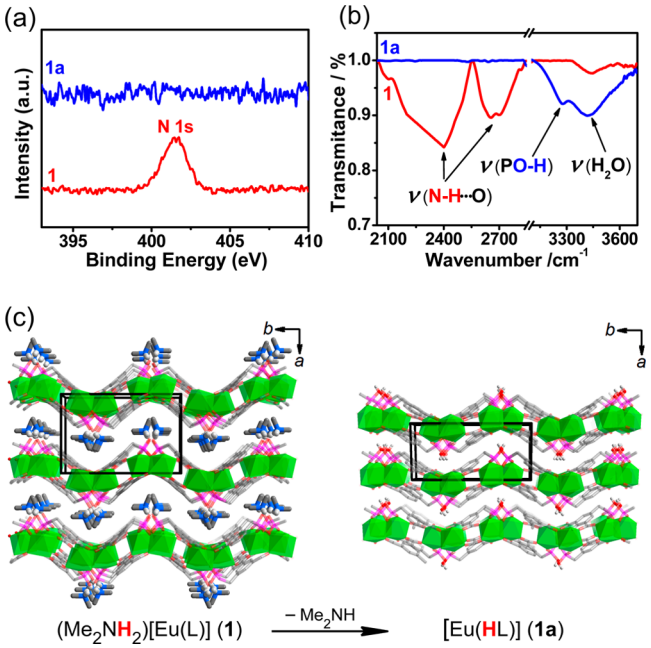

Figure 4. (a) High-resolution XPS spectra of N 1s. (b) IR spectra. (c) Proton transfer from an anionic structure to an identical neutral structure induced by removal of Me_2NH molecules.

A precise single-crystal structure of the final phase [Eu(HL)] (**1a**) after proton transfer from $(Me_2NH_2)^+$ cations to the O_3P group provides the most convincing evidence. SCSC transformations are highly desirable to identify the structural changes observed with single-crystal X-ray crystallography.[32] Taking advantage of the high thermal stability of **1a**, we successfully prepared high-quality single crystals by an extremely slow heat-treatment process. Crystal data: space group $P2_1/c$, a = 7.9655(5) Å, b = 15.6161(9) Å, c = 9.2917(6) Å, β = 112.201(2)°, V = 1070.11(12) Å^3 (Table S7). Crystal structure analysis of [Eu(HL)] (**1a**) showed that while it retains the original space group and metal−ligand connectivity of the 2D host framework of (Me_2NH_2)[Eu(L)] (**1**), the interlayer Me_2NH^+ counterions have been completely removed (Figures 4c and S27−S29). This resulted in over −25% and −21% shrinkages of the unit-cell volume and length of the a-axis, respectively, together with small changes of the b (+2.3%) and c (< −1%) axes (Figure S29 and Table S7). In view of the fact that removal of Me_2NH molecules resulted in attachment of protons to O atoms of phosphoric groups, SCSC transformation occurs from a cationic sandwich type MOF (Me_2NH_2)[Eu(HL)] to a closely packed neutral one [Eu(**H**L)] thermally accompanied by proton transfer. To our best knowledge, there are few comprehensive reports on this kind of structure transformation,[8d,33] even through the literature contains a large number of transformations based on studies of the initial and final structures.[4g,25b,32b,34]

Obviously, comparison of the proton conductivities of **1a** with that of **1** can be utilized to examine the role that the hydrogen-bonded chains play during proton transfer. Nevertheless, due to poor crystallinity of the large single crystals of **1a**, AC impedance measurements could not be carried out. However, measurements conducted on a compacted pellet of **1a** under high humidity conditions indicate that the proton conductivity of **1a** falls sharply (5.29×10^{-5} S·cm^{-1} at 100 °C, 98% RH), being far less than that of **1** (3.76×10^{-3} S·cm^{-1} at 100 °C, 98% RH), which implies that the strongly hydrogen-bonded chains in **1** may facilitate transfer of protons (Figures 5a and S18). The calculated activation energy (1.50 eV) suggests that **1a** requires a large number of water molecules to serve as carriers to transport protons according to the vehicle mechanism (> 0.4 eV) (Figure 5b). Therefore, a conclusion can be drawn that the hydrogen-bonded chains of **1** really play a vital role on fast proton transfer.

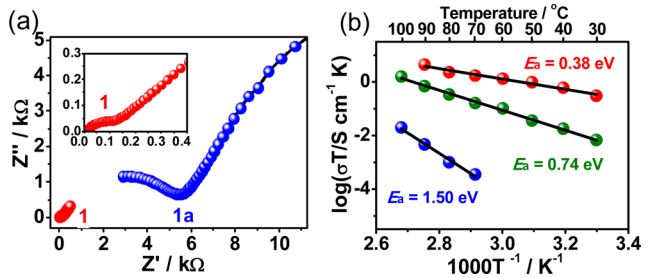

Figure 5. (a) Nyquist plots of **1** and **1a** at 100 °C and 98% RH. (b) Arrhenius plots for bulk (red) and grain-boundary (green) conductivities of **1** and Arrhenius plot of proton conductivity of **1a** (blue); the linear fits are shown as black lines.

Reversible Proton Transfer Verified by Luminescence Properties. To better understand the role of strongly hydrogen-bonded chains (N−H···O) in the structure−property relationship of structure **1**, its temperature-dependent photoluminescence properties were investigated. With increasing

DOI: 10.1021/jacs.6b12847
J. Am. Chem. Soc. 2017, 139, 3505−3512

temperatures from 25 to 150 °C, the intensity of the characteristic red emission of Eu(III) corresponding to the $^5D_0 \rightarrow {}^7F_2$ transition (609 nm) remained steady and then showed a slight decrease before reaching 300 °C, which arises from radiative relaxation of the excited-state energy-induced high temperatures. Upon further heating, emission intensity gradually declined until it completely disappeared at 450 °C, which could not be recovered by cooling back to room temperature (Figure 6a,b). These observations suggest that

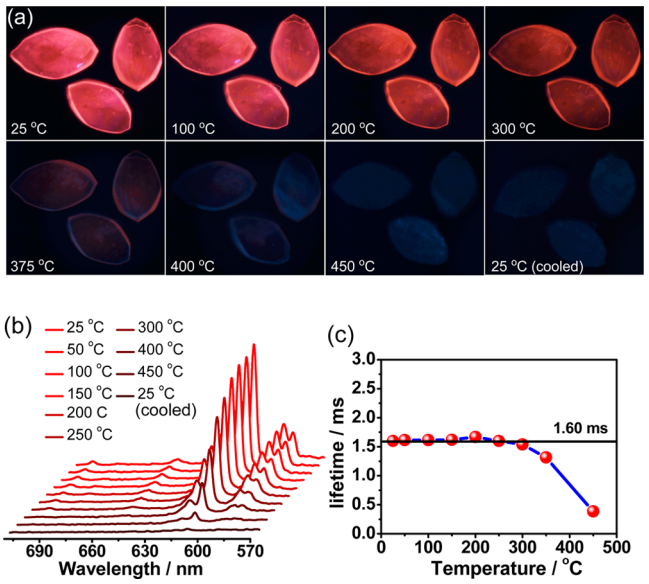

Figure 6. (a) Photoluminescence microscopic images of **1** at different temperatures. (b) Emission spectra of **1** recorded from 25 to 450 °C and then cooled to 25 °C (excitation at 394 nm). (c) Decay lifetimes of $^5D_0 \rightarrow {}^7F_2$ transition of **1** with emission monitored at 609 nm (λ_{ex} = 394 nm) at room-temperature after being heated at different temperatures under N_2 for 30 min.

irreversible changes happened in the structural transformation from **1** to **1a**. Besides this, room-temperature lifetime measurements of samples of **1** after different temperature treatments showed that the lifetime of the $^5D_0$ excited state is almost unchanged (~1.60 ms) from 25 to 300 °C but drops sharply (0.39 ms) when heated continuously (Figures 6c and S30, and Table S6), which coincides with the process of Me_2NH removal (Figures 2a, S7, and S25). Considering that vibronic coupling with O−H can effectively quench the excited state of lanthanide-based MOFs,[13b,35] the present observation of luminescence quenching and shortened lifetime prompted us to conclude that formation of O−H in **1a** occurred after removal of deprotonated Me_2NH molecules from the $(Me_2NH_2)^+$ cations.

To further verify whether the protons can reversibly hop among the acid−base pairs, experimental conversion of **1a** back to **1** was carried out. When a sample of **1a** was heat-treated in a Me_2NH aqueous solution, its luminescence intensities partially recovered (Figures S31 and S32). In addition, the PXRD pattern and IR of this prepared sample (**1′**) agreed very well with those of **1** (Figures S5 and S32). In particular, after persistent attempts, we were able to determine the single-crystal structure of **1′** (Table S7) and demonstrate its similarity to that of **1**, which lent further support to the idea that Me_2NH molecules could penetrate the interfacial layer of **1a** and finally recapture the protons from the protonated phosphate groups to form $(Me_2NH_2)^+$ cations (Figures S5, S31, and S32). In other words, reversible proton-hopping between the $(Me_2NH_2)^+$ cations and phosphate groups along the hydrogen-bonded chains has been successfully realized, which can sufficiently demonstrate the importance of a continuous passageway in the hydrogen-bonding chain for proton conduction and deepens our understanding of the proton-transfer mechanism in MOFs.

CONCLUSION

In summary, we have successfully synthesized a new acid−base pair proton-conducting MOF, which features highly ordered strongly hydrogen-bonded chains between counter cations $(Me_2NH_2)^+$ and phosphonate groups of the anionic host framework. This new crystalline material exhibits remarkable anhydrous conductivity along hydrogen-bonded (N−H···O) chains, and water-assisted proton conductivity in a powder pellet. More importantly, by virtue of the excellent single crystallinity of the material at high temperature, the proton transfer mechanism was well elucidated by a series of in situ variable-temperature characterization methods, as well as controlled experiments including SCSC transformation accompanied by proton transfer between an anionic framework and an identical neutral framework. The comprehensive study demonstrated unique proton vibration and transfer among acid−base pairs within hydrogen-bonded (N−H···O) chains via electrostatic interactions. To our best knowledge, there exist very few reports of highly effective proton conductors that can provide such direct visualization of proton dynamical behavior. We believe that this work can be instructive for further exploration of new proton conductive materials and even point the way to improvements of efficient proton sensors.

ASSOCIATED CONTENT

Supporting Information

The Supporting Information is available free of charge on the ACS Publications website at DOI: 10.1021/jacs.6b12847.

Experimental procedures and PXRD, IR, TGA, DSC, XPS, proton conductivity, H_2/O_2 fuel cell, and photoluminescence measurements (PDF)

CIF data (ZIP)

AUTHOR INFORMATION

Corresponding Author

*E-mail: zangsqzg@zzu.edu.cn.

ORCID

Shuang-Quan Zang: 0000-0002-6728-0559

Thomas C. W. Mak: 0000-0002-4316-2937

Notes

The authors declare no competing financial interest.

ACKNOWLEDGMENTS

This work was supported by the National Natural Science Foundation of China (nos. 21601157, 21501046, 21371153, 21671175), the Program for Science & Technology Innovation Talents in Universities of Henan Province (164100510005), and Zhengzhou University. We are grateful to Prof. S.-F. Lu of Beihang University for the H_2/O_2 fuel cell measurements.

DOI: 10.1021/jacs.6b12847
J. Am. Chem. Soc. 2017, 139, 3505−3512

REFERENCES

(1) (a) Scofield, M. E.; Liu, H.; Wong, S. S. *Chem. Soc. Rev.* **2015**, *44*, 5836−5860. (b) Kreuer, K.-D.; Paddison, S. J.; Spohr, E.; Schuster, M. *Chem. Rev.* **2004**, *104*, 4637−4678.

(2) (a) Jiang, J.; Furukawa, H.; Zhang, Y.-B.; Yaghi, O. M. *J. Am. Chem. Soc.* **2016**, *138*, 10244−10251. (b) Cui, X.; Chen, K.; Xing, H.; Yang, Q.; Krishna, R.; Bao, Z.; Wu, H.; Zhou, W.; Dong, X.; Han, Y.; Li, B.; Ren, Q.; Zaworotko, M. J.; Chen, B. *Science* **2016**, *353*, 141. (c) Chen, K.-J.; Scott, H. S.; Madden, D. G.; Pham, T.; Kumar, A.; Bajpai, A.; Lusi, M.; Forrest, K. A.; Space, B.; Perry, J. J.; Zaworotko, M. J. *Chem.* **2016**, *1*, 753−765. (d) Savage, M.; da Silva, I.; Johnson, M.; Carter, J. H.; Newby, R.; Suyetin, M.; Besley, E.; Manuel, P.; Rudić, S.; Fitch, A. N.; Murray, C.; David, W. I. F.; Yang, S.; Schröder, M. *J. Am. Chem. Soc.* **2016**, *138*, 9119−9127. (e) Ding, N.; Li, H.; Feng, X.; Wang, Q.; Wang, S.; Ma, L.; Zhou, J.; Wang, B. *J. Am. Chem. Soc.* **2016**, *138*, 10100−10103. (f) Sung Cho, H.; Deng, H.; Miyasaka, K.; Dong, Z.; Cho, M.; Neimark, A. V.; Ku Kang, J.; Yaghi, O. M.; Terasaki, O. *Nature* **2015**, *527*, 503−507. (g) Tu, B.; Pang, Q.; Ning, E.; Yan, W.; Qi, Y.; Wu, D.; Li, Q. *J. Am. Chem. Soc.* **2015**, *137*, 13456−13459. (h) Guillerm, V.; Weseliński, L. J.; Belmabkhout, Y.; Cairns, A. J.; D'Elia, V.; Wojtas, L.; Adil, K.; Eddaoudi, M. *Nat. Chem.* **2014**, *6*, 673−680. (i) Chen, B.; Eddaoudi, M.; Hyde, S. T.; O'Keeffe, M.; Yaghi, O. M. *Science* **2001**, *291*, 1021−1023.

(3) (a) Huang, R.-W.; Wei, Y.-S.; Dong, X.-Y.; Wu, X.-H.; Du, C.-X.; Zang, S.-Q.; Mak, T. C. W. *Nat. Chem.* **2017**, DOI: 10.1038/nchem.2718. (b) Lin, R.-B.; Liu, S.-Y.; Ye, J.-W.; Li, X.-Y.; Zhang, J.-P. *Adv. Sci.* **2016**, *3*, 1500434. (c) Gong, Q.; Hu, Z.; Deibert, B. J.; Emge, T. J.; Teat, S. J.; Banerjee, D.; Mussman, B.; Rudd, N. D.; Li, J. *J. Am. Chem. Soc.* **2014**, *136*, 16724−16727. (d) Shustova, N. B.; Cozzolino, A. F.; Reineke, S.; Baldo, M.; Dincă, M. *J. Am. Chem. Soc.* **2013**, *135*, 13326−13329. (e) Kang, Y.; Wang, F.; Zhang, J.; Bu, X. *J. Am. Chem. Soc.* **2012**, *134*, 17881−17884. (f) Takashima, Y.; Martínez, V. M.; Furukawa, S.; Kondo, M.; Shimomura, S.; Uehara, H.; Nakahama, M.; Sugimoto, K.; Kitagawa, S. *Nat. Commun.* **2011**, *2*, 168.

(4) (a) Fracaroli, A. M.; Siman, P.; Nagib, D. A.; Suzuki, M.; Furukawa, H.; Toste, F. D.; Yaghi, O. M. *J. Am. Chem. Soc.* **2016**, *138*, 8352−8355. (b) Yu, X.; Cohen, S. M. *J. Am. Chem. Soc.* **2016**, *138*, 12320−12323. (c) Grigoropoulos, A.; Whitehead, G. F. S.; Perret, N.; Katsoulidis, A. P.; Chadwick, F. M.; Davies, R. P.; Haynes, A.; Brammer, L.; Weller, A. S.; Xiao, J.; Rosseinsky, M. J. *Chem. Sci.* **2016**, *7*, 2037−2050. (d) Wang, X.; Han, X.; Zhang, J.; Wu, X.; Liu, Y.; Cui, Y. *J. Am. Chem. Soc.* **2016**, *138*, 12332−12335. (e) Johnson, J. A.; Petersen, B. M.; Kormos, A.; Echeverría, E.; Chen, Y.-S.; Zhang, J. *J. Am. Chem. Soc.* **2016**, *138*, 10293−10298. (f) Zhou, Z.; He, C.; Xiu, J.; Yang, L.; Duan, C. *J. Am. Chem. Soc.* **2015**, *137*, 15066−15069. (g) Wei, Y.-S.; Zhang, M.; Liao, P.-Q.; Lin, R.-B.; Li, T.-Y.; Shao, G.; Zhang, J.-P.; Chen, X.-M. *Nat. Commun.* **2015**, *6*, 8348.

(5) (a) Jiang, J.; Zhao, Y.; Yaghi, O. M. *J. Am. Chem. Soc.* **2016**, *138*, 3255−3265. (b) Schoedel, A.; Li, M.; Li, D.; O'Keeffe, M.; Yaghi, O. M. *Chem. Rev.* **2016**, *116*, 12466−12535. (c) Howarth, A. J.; Liu, Y.; Li, P.; Li, Z.; Wang, T. C.; Hupp, J. T.; Farha, O. K. *Nat. Rev. Mater.* **2016**, *1*, 15018. (d) Cui, Y.; Li, B.; He, H.; Zhou, W.; Chen, B.; Qian, G. *Acc. Chem. Res.* **2016**, *49*, 483−493. (e) Murray, L. J.; Dinca, M.; Long, J. R. *Chem. Soc. Rev.* **2009**, *38*, 1294−1314. (f) Zacher, D.; Shekhah, O.; Woll, C.; Fischer, R. A. *Chem. Soc. Rev.* **2009**, *38*, 1418−1429. (g) Kitagawa, S.; Kitaura, R.; Noro, S.-i. *Angew. Chem., Int. Ed.* **2004**, *43*, 2334−2375.

(6) (a) Meng, X.; Wang, H.-N.; Song, S.-Y.; Zhang, H.-J. *Chem. Soc. Rev.* **2017**, *46*, 464−480. (b) Sadakiyo, M.; Yamada, T.; Kitagawa, H. *ChemPlusChem* **2016**, *81*, 691−701. (c) Ramaswamy, P.; Wong, N. E.; Shimizu, G. K. H. *Chem. Soc. Rev.* **2014**, *43*, 5913−5932. (d) Yoon, M.; Suh, K.; Natarajan, S.; Kim, K. *Angew. Chem., Int. Ed.* **2013**, *52*, 2688−2700. (e) Horike, S.; Umeyama, D.; Kitagawa, S. *Acc. Chem. Res.* **2013**, *46*, 2376−2384.

(7) (a) Khatua, S.; Kumar Bar, A.; Konar, S. *Chem. - Eur. J.* **2016**, *22*, 16277−16285. (b) Nguyen, N. T. T.; Furukawa, H.; Gándara, F.; Trickett, C. A.; Jeong, H. M.; Cordova, K. E.; Yaghi, O. M. *J. Am. Chem. Soc.* **2015**, *137*, 15394−15397. (c) Zhai, Q.-G.; Mao, C.; Zhao, X.; Lin, Q.; Bu, F.; Chen, X.; Bu, X.; Feng, P. *Angew. Chem., Int. Ed.* **2015**, *54*, 7886−7890. (d) Meng, X.; Song, S.-Y.; Song, X.-Z.; Zhu, M.; Zhao, S.-N.; Wu, L.-L.; Zhang, H.-J. *Chem. Commun.* **2015**, *51*, 8150−8152. (e) Dong, X.-Y.; Wang, R.; Wang, J.-Z.; Zang, S.-Q.; Mak, T. C. W. *J. Mater. Chem. A* **2015**, *3*, 641−647. (f) Phang, W. J.; Lee, W. R.; Yoo, K.; Ryu, D. W.; Kim, B.; Hong, C. S. *Angew. Chem., Int. Ed.* **2014**, *53*, 8383−8387. (g) Panda, T.; Kundu, T.; Banerjee, R. *Chem. Commun.* **2013**, *49*, 6197−6199.

(8) (a) Borges, D. D.; Devautour-Vinot, S.; Jobic, H.; Ollivier, J.; Nouar, F.; Semino, R.; Devic, T.; Serre, C.; Paesani, F.; Maurin, G. *Angew. Chem., Int. Ed.* **2016**, *55*, 3919−3924. (b) Taylor, J. M.; Komatsu, T.; Dekura, S.; Otsubo, K.; Takata, M.; Kitagawa, H. *J. Am. Chem. Soc.* **2015**, *137*, 11498−11506. (c) Phang, W. J.; Jo, H.; Lee, W. R.; Song, J. H.; Yoo, K.; Kim, B.; Hong, C. S. *Angew. Chem., Int. Ed.* **2015**, *54*, 5142−5146. (d) Bao, S.-S.; Otsubo, K.; Taylor, J. M.; Jiang, Z.; Zheng, L.-M.; Kitagawa, H. *J. Am. Chem. Soc.* **2014**, *136*, 9292−9295. (e) Taylor, J. M.; Dawson, K. W.; Shimizu, G. K. H. *J. Am. Chem. Soc.* **2013**, *135*, 1193−1196. (f) Liang, X.; Zhang, F.; Feng, W.; Zou, X.; Zhao, C.; Na, H.; Liu, C.; Sun, F.; Zhu, G. *Chem. Sci.* **2013**, *4*, 983−992.

(9) (a) Neville, S. M.; Halder, G. J.; Chapman, K. W.; Duriska, M. B.; Moubaraki, B.; Murray, K. S.; Kepert, C. J. *J. Am. Chem. Soc.* **2009**, *131*, 12106−12108. (b) McManus, G. J.; Perry, J. J.; Perry, M.; Wagner, B. D.; Zaworotko, M. J. *J. Am. Chem. Soc.* **2007**, *129*, 9094−9101.

(10) (a) Inukai, M.; Horike, S.; Itakura, T.; Shinozaki, R.; Ogiwara, N.; Umeyama, D.; Nagarkar, S.; Nishiyama, Y.; Malon, M.; Hayashi, A.; Ohhara, T.; Kiyanagi, R.; Kitagawa, S. *J. Am. Chem. Soc.* **2016**, *138*, 8505−8511. (b) Ye, Y.; Wu, X.; Yao, Z.; Wu, L.; Cai, Z.; Wang, L.; Ma, X.; Chen, Q.-H.; Zhang, Z.; Xiang, S. *J. Mater. Chem. A* **2016**, *4*, 4062−4070. (c) Luo, H.-B.; Ren, L.-T.; Ning, W.-H.; Liu, S.-X.; Liu, J.-L.; Ren, X.-M. *Adv. Mater.* **2016**, *28*, 1663−1667. (d) Ma, H.; Liu, B.; Li, B.; Zhang, L.; Li, Y.-G.; Tan, H.-Q.; Zang, H.-Y.; Zhu, G. *J. Am. Chem. Soc.* **2016**, *138*, 5897−5903. (e) Ponomareva, V. G.; Kovalenko, K. A.; Chupakhin, A. P.; Dybtsev, D. N.; Shutova, E. S.; Fedin, V. P. *J. Am. Chem. Soc.* **2012**, *134*, 15640−15643. (f) Umeyama, D.; Horike, S.; Inukai, M.; Hijikata, Y.; Kitagawa, S. *Angew. Chem., Int. Ed.* **2011**, *50*, 11706−11709. (g) Hurd, J. A.; Vaidhyanathan, R.; Thangadurai, V.; Ratcliffe, C. I.; Moudrakovski, I. L.; Shimizu, G. K. H. *Nat. Chem.* **2009**, *1*, 705−710. (h) Bureekaew, S.; Horike, S.; Higuchi, M.; Mizuno, M.; Kawamura, T.; Tanaka, D.; Yanai, N.; Kitagawa, S. *Nat. Mater.* **2009**, *8*, 831−836.

(11) Nagarkar, S. S.; Unni, S. M.; Sharma, A.; Kurungot, S.; Ghosh, S. K. *Angew. Chem., Int. Ed.* **2014**, *53*, 2638−2642.

(12) Liu, M.; Chen, L.; Lewis, S.; Chong, S. Y.; Little, M. A.; Hasell, T.; Aldous, I. M.; Brown, C. M.; Smith, M. W.; Morrison, C. A.; Hardwick, L. J.; Cooper, A. I. *Nat. Commun.* **2016**, *7*, 12750.

(13) (a) Bao, S.-S.; Li, N.-Z.; Taylor, J. M.; Shen, Y.; Kitagawa, H.; Zheng, L.-M. *Chem. Mater.* **2015**, *27*, 8116−8125. (b) Tang, Q.; Liu, Y.; Liu, S.; He, D.; Miao, J.; Wang, X.; Yang, G.; Shi, Z.; Zheng, Z. *J. Am. Chem. Soc.* **2014**, *136*, 12444−12449. (c) Zhao, X.; Mao, C.; Bu, X.; Feng, P. *Chem. Mater.* **2014**, *26*, 2492−2495. (d) Umeyama, D.; Horike, S.; Inukai, M.; Itakura, T.; Kitagawa, S. *J. Am. Chem. Soc.* **2012**, *134*, 12780−12785. (e) Qin, L.; Yu, Y.-Z.; Liao, P.-Q.; Xue, W.; Zheng, Z.; Chen, X.-M.; Zheng, Y.-Z. *Adv. Mater.* **2016**, *28*, 10772−10779.

(14) O'Keeffe, M.; Peskov, M. A.; Ramsden, S. J.; Yaghi, O. M. *Acc. Chem. Res.* **2008**, *41*, 1782−1789.

(15) (a) Shi, F.-N.; Cunha-Silva, L.; Trindade, T.; Paz, F. A. A.; Rocha, J. *Cryst. Growth Des.* **2009**, *9*, 2098−2109. (b) Gremlich, H.-U. *Infrared and Raman Spectroscopy, Ullmann's Encyclopedia of Industrial Chemistry*; John Wiley: New York, 2000. (c) Hachuła, B.; Flakus, H. T.; Garbacz, A.; Stolarczyk, A. *Spectrochim. Acta, Part A* **2014**, *123*, 151−157. (d) Liao, W.-M.; Shi, H.-T.; Shi, X.-H.; Yin, Y.-G. *Dalton Trans.* **2014**, *43*, 15305−15307. (e) Cui, X.; Xu, M.-C.; Zhang, L.-J.; Yao, R.-X.; Zhang, X.-M. *Dalton Trans.* **2015**, *44*, 12711−12716. (f) Chen, Z.; Ling, Y.; Yang, H.; Guo, Y.; Weng, L.; Zhou, Y. *CrystEngComm* **2011**, *13*, 3378−3382.

(16) Tu, T. N.; Phan, N. Q.; Vu, T. T.; Nguyen, H. L.; Cordova, K. E.; Furukawa, H. *J. Mater. Chem. A* **2016**, *4*, 3638−3641.

DOI: 10.1021/jacs.6b12847
J. Am. Chem. Soc. 2017, 139, 3505−3512

(17) Wang, C.; Liu, X.; Keser Demir, N.; Chen, J. P.; Li, K. *Chem. Soc. Rev.* **2016**, *45*, 5107−5134.
(18) Horike, S.; Umeyama, D.; Inukai, M.; Itakura, T.; Kitagawa, S. *J. Am. Chem. Soc.* **2012**, *134*, 7612−7615.
(19) Horike, S.; Chen, W.; Itakura, T.; Inukai, M.; Umeyama, D.; Asakura, H.; Kitagawa, S. *Chem. Commun.* **2014**, *50*, 10241−10243.
(20) Umeyama, D.; Horike, S.; Inukai, M.; Kitagawa, S. *J. Am. Chem. Soc.* **2013**, *135*, 11345−11350.
(21) (a) Barsoukov, E.; Macdonald, J. R. *Impedance Spectroscopy: Theory, Experiment, and Applications*, 2nd ed.; John Wiley & Sons, Inc., 2005. (b) Ogiwara, N.; Inukai, M.; Itakura, T.; Horike, S.; Kitagawa, S. *Chem. Mater.* **2016**, *28*, 3968−3975.
(22) Dong, X.-Y.; Wang, R.; Li, J.-B.; Zang, S.-Q.; Hou, H.-W.; Mak, T. C. W. *Chem. Commun.* **2013**, *49*, 10590−10592.
(23) Kim, S.; Dawson, K. W.; Gelfand, B. S.; Taylor, J. M.; Shimizu, G. K. H. *J. Am. Chem. Soc.* **2013**, *135*, 963−966.
(24) Kang, D. W.; Lim, K. S.; Lee, K. J.; Lee, J. H.; Lee, W. R.; Song, J. H.; Yeom, K. H.; Kim, J. Y.; Hong, C. S. *Angew. Chem., Int. Ed.* **2016**, *55*, 16123−16126.
(25) (a) Pang, J.; Liu, C.; Huang, Y.; Wu, M.; Jiang, F.; Yuan, D.; Hu, F.; Su, K.; Liu, G.; Hong, M. *Angew. Chem.* **2016**, *128*, 7604−7608. (b) Wei, Y.-S.; Chen, K.-J.; Liao, P.-Q.; Zhu, B.-Y.; Lin, R.-B.; Zhou, H.-L.; Wang, B.-Y.; Xue, W.; Zhang, J.-P.; Chen, X.-M. *Chem. Sci.* **2013**, *4*, 1539−1546. (c) Goodwin, A. L.; Calleja, M.; Conterio, M. J.; Dove, M. T.; Evans, J. S. O.; Keen, D. A.; Peters, L.; Tucker, M. G. *Science* **2008**, *319*, 794.
(26) (a) Huang, Y.-G.; Shiota, Y.; Su, S.-Q.; Wu, S.-Q.; Yao, Z.-S.; Li, G.-L.; Kanegawa, S.; Kang, S.; Kamachi, T.; Yoshizawa, K.; Ariga, K.; Sato, O. *Angew. Chem., Int. Ed.* **2016**, *55*, 14628−14632. (b) Zhou, H.-L.; Zhang, Y.-B.; Zhang, J.-P.; Chen, X.-M. *Nat. Commun.* **2015**, *6*, 6917. (c) Zhou, H.-L.; Lin, R.-B.; He, C.-T.; Zhang, Y.-B.; Feng, N.; Wang, Q.; Deng, F.; Zhang, J.-P.; Chen, X.-M. *Nat. Commun.* **2013**, *4*, 2534.
(27) (a) Lee, S.; Kapustin, E. A.; Yaghi, O. M. *Science* **2016**, *353*, 808. (b) Liao, P.-Q.; Zhang, W.-X.; Zhang, J.-P.; Chen, X.-M. *Nat. Commun.* **2015**, *6*, 8697. (c) Bloch, W. M.; Burgun, A.; Coghlan, C. J.; Lee, R.; Coote, M. L.; Doonan, C. J.; Sumby, C. J. *Nat. Chem.* **2014**, *6*, 906−912. (d) Kubota, R.; Tashiro, S.; Shiro, M.; Shionoya, M. *Nat. Chem.* **2014**, *6*, 913−918. (e) Ikemoto, K.; Inokuma, Y.; Rissanen, K.; Fujita, M. *J. Am. Chem. Soc.* **2014**, *136*, 6892−6895. (f) Inokuma, Y.; Kawano, M.; Fujita, M. *Nat. Chem.* **2011**, *3*, 349−358.
(28) (a) Horiuchi, S.; Kumai, R.; Tokura, Y. *Angew. Chem., Int. Ed.* **2007**, *46*, 3497−3501. (b) Wilson, C. C.; Goeta, A. E. *Angew. Chem., Int. Ed.* **2004**, *43*, 2095−2099. (c) Gilli, P.; Bertolasi, V.; Pretto, L.; Antonov, L.; Gilli, G. *J. Am. Chem. Soc.* **2005**, *127*, 4943−4953. (d) Rybarczyk-Pirek, A. J. *Struct. Chem.* **2012**, *23*, 1739−1749. (e) Parkin, A.; Wozniak, K.; Wilson, C. C. *Cryst. Growth Des.* **2007**, *7*, 1393−1398.
(29) (a) Yang, D.; Bernales, V.; Islamoglu, T.; Farha, O. K.; Hupp, J. T.; Cramer, C. J.; Gagliardi, L.; Gates, B. C. *J. Am. Chem. Soc.* **2016**, *138*, 15189−15196. (b) Planas, N.; Mondloch, J. E.; Tussupbayev, S.; Borycz, J.; Gagliardi, L.; Hupp, J. T.; Farha, O. K.; Cramer, C. J. *J. Phys. Chem. Lett.* **2014**, *5*, 3716−3723. (c) Garrone, E.; Otero Arean, C. *Chem. Soc. Rev.* **2005**, *34*, 846−857. (d) Lamberti, C.; Zecchina, A.; Groppo, E.; Bordiga, S. *Chem. Soc. Rev.* **2010**, *39*, 4951−5001.
(30) (a) Zhang, K.; Nelson, A. M.; Talley, S. J.; Chen, M.; Margaretta, E.; Hudson, A. G.; Moore, R. B.; Long, T. E. *Green Chem.* **2016**, *18*, 4667−4681. (b) Merino, D. H.; Slark, A. T.; Colquhoun, H. M.; Hayes, W.; Hamley, I. W. *Polym. Chem.* **2010**, *1*, 1263−1271. (c) Coleman, M. M.; Lee, K. H.; Skrovanek, D. J.; Painter, P. C. *Macromolecules* **1986**, *19*, 2149−2157.
(31) (a) Vilela, S. M. F.; Fernandes, J. A.; Ananias, D.; Carlos, L. D.; Rocha, J.; Tome, J. P. C.; Almeida Paz, F. A. *CrystEngComm* **2014**, *16*, 344−358. (b) Vilela, S. M. F.; Ananias, D.; Gomes, A. C.; Valente, A. A.; Carlos, L. D.; Cavaleiro, J. A. S.; Rocha, J.; Tome, J. P. C.; Almeida Paz, F. A. *J. Mater. Chem.* **2012**, *22*, 18354−18371.
(32) (a) Chang, Z.; Yang, D.-H.; Xu, J.; Hu, T.-L.; Bu, X.-H. *Adv. Mater.* **2015**, *27*, 5432−5441. (b) Zhang, J.-P.; Liao, P.-Q.; Zhou, H.-L.; Lin, R.-B.; Chen, X.-M. *Chem. Soc. Rev.* **2014**, *43*, 5789−5814. (c) Kitagawa, S.; Uemura, K. *Chem. Soc. Rev.* **2005**, *34*, 109−119. (d) Kole, G. K.; Vittal, J. J. *Chem. Soc. Rev.* **2013**, *42*, 1755−1775. (e) Medishetty, R.; Park, I.-H.; Lee, S. S.; Vittal, J. J. *Chem. Commun.* **2016**, *52*, 3989−4001.
(33) (a) Gelfand, B. S.; Huynh, R. P. S.; Mah, R. K.; Shimizu, G. K. H. *Angew. Chem., Int. Ed.* **2016**, *55*, 14614−14617. (b) Cai, Z.-S.; Bao, S.-S.; Wang, X.-Z.; Hu, Z.; Zheng, L.-M. *Inorg. Chem.* **2016**, *55*, 3706−3712.
(34) (a) Ferguson, A.; Liu, L.; Tapperwijn, S. J.; Perl, D.; Coudert, F.-X.; Van Cleuvenbergen, S.; Verbiest, T.; van der Veen, M. A.; Telfer, S. G. *Nat. Chem.* **2016**, *8*, 250−257. (b) Yuan, S.; Chen, Y.-P.; Qin, J.-S.; Lu, W.; Zou, L.; Zhang, Q.; Wang, X.; Sun, X.; Zhou, H.-C. *J. Am. Chem. Soc.* **2016**, *138*, 8912−8919. (c) Chen, C.-X.; Wei, Z.; Jiang, J.-J.; Fan, Y.-Z.; Zheng, S.-P.; Cao, C.-C.; Li, Y.-H.; Fenske, D.; Su, C.-Y. *Angew. Chem., Int. Ed.* **2016**, *55*, 9932−9936. (d) Marshall, R. J.; Griffin, S. L.; Wilson, C.; Forgan, R. S. *J. Am. Chem. Soc.* **2015**, *137*, 9527−9530. (e) Cao, L.-H.; Wei, Y.-S.; Xu, H.; Zang, S.-Q.; Mak, T. C. W. *Adv. Funct. Mater.* **2015**, *25*, 6448−6457. (f) Dong, X.-Y.; Li, B.; Ma, B.-B.; Li, S.-J.; Dong, M.-M.; Zhu, Y.-Y.; Zang, S.-Q.; Song, Y.; Hou, H.-W.; Mak, T. C. W. *J. Am. Chem. Soc.* **2013**, *135*, 10214−10217. (g) Zhang, Z.; Wojtas, L.; Eddaoudi, M.; Zaworotko, M. J. *J. Am. Chem. Soc.* **2013**, *135*, 5982−5985.
(35) (a) Horrocks, W. D.; Sudnick, D. R. *J. Am. Chem. Soc.* **1979**, *101*, 334−340. (b) Chen, B.; Wang, L.; Zapata, F.; Qian, G.; Lobkovsky, E. B. *J. Am. Chem. Soc.* **2008**, *130*, 6718−6719. (c) Wong, K. L.; Law, G. L.; Yang, Y. Y.; Wong, W. T. *Adv. Mater.* **2006**, *18*, 1051−1054. (d) Yu, Y.; Zhang, X.-M.; Ma, J.-P.; Liu, Q.-K.; Wang, P.; Dong, Y.-B. *Chem. Commun.* **2014**, *50*, 1444−1446.

DOI: 10.1021/jacs.6b12847
J. Am. Chem. Soc. 2017, 139, 3505−3512